CFD analysis on the freefall of a lifeboat

Mateus Fujita Silveira
Instituto Superior Técnico, Lisbon, Portugal

ABSTRACT: Slamming loads on lifeboats is studied in this study by using the open source CFD toolbox OpenFOAM. For this purpose, the overset grid technic is used to perform multiphase simulations, based on the volume of fluid method, due to the large motion that is expected from this kind of formulation. After reviewing the slamming research until nowadays and make an overview over the software OpenFOAM and chimera mesh method, a validation study was made by comparing the assessment of the water entry of a 30° deadrise angle wedge with experimental results obtained from other studies. The results were in good agreement not only with the measurements, but also with the boundary element method numerical results and deforming mesh simulations that were published before. As for the lifeboat simulations, they have shown to be more demanding of computer capacity, but still a robust tool for this purpose. Totally 21 different simulations were performed by using 7 different initial pitch angles and 3 different dropping heights. The pressure over several points in the same transversal and longitudinal plan were compared. As for the pressures, it was noticed that two major peaks occur: one on the bow during water entry and other on the stern, that appears after a second water entry due to the turnback spin induced by restoring moments. The pressure contours have shown that the keel of the lifeboat is the critical part with the highest loads. The kinematics were also compared to check which angle would be able to get further from the hazardous event without any more impulse. In this aspect, the launching with an initial pitch angle of 70° presented the best performance for a wide range of heights.

1 INTRODUCTION

The safety of life in sea should be guaranteed for a ship to navigate. One way to secure this during extreme maritime incidents where the crew and persons on board must leave the ship is by having and using lifeboats. This kind of boat is required to be launched from a ship deck or a platform from a considerable height, gaining enough momentum and saving launch time. In this scenario, the lifeboat experiences a free-fall process before approaching the water surface, entering with high speed, and causing significant pressure forces on the lifeboat structure, and if the boat is launched or designed incorrectly, the structure can be compromised causing serious damage to the hull structure and threaten the personal safety of the crew (Qiu, et al., 2020). Therefore, it is essential to assess the water entry impacts and prepare accordingly during the lifeboat design circles (Huang, et al., 2021).

Assessing the water entry impact, however, is a challenge even nowadays. The most reliable method to study and evaluate this is by performing experiments, but it is unrealistic to measure the pressure this way since it would be necessary to cover all the hull sensitive areas with pressure sensors and it would limit the locations where these measurements can be taken. This is why several alternatives are in development, such as finite element analysis models together with CFD simulations, computational models, etc, but are also still improving and requiring validation from the existing experimental known results.

As an important application in naval architecture, the dynamic variation of pressure on surface ships and offshore structures during the water entry process has been a long-lasting topic. The pioneering study is attributed by Von Karman (1929), who aimed to develop a method capable of obtaining the impact force on a seaplane landing on water surface by proposing the application of momentum variation to compute the hydrodynamic force acting on a bluff body penetrating liquid surface. This depends on the speed rate and wetted area. Later on, Wagner (1932) established another groundwork by developing the theoretical models on the idealized problem of a two-dimensional wedge entering the water and assuming it to rise as jet flows and hit on the walls of the wedge, to have irrotational flow and applicable for linear boundary conditions neglecting gravity (Huang, et al., 2021; Shen, et al., 2016). Wagner's asymptotic solution has gone through adaptations, and it is applied to various research and practical conditions. It can be applied for obtaining the water entry loads and coupling them with structural solution, but it also neglects some hydrodynamic phenomena, causing the modelled flow field to be unrealistic. One example of these phenomena is the flow separation that typically occurs for wedge bodies.

Later on, Zhao and Faltinsen (1993) developed a numerical method for studying water entry of a two-dimensional body of arbitrary cross-section which relies on the panel method with potential flow theory to obtain the Froude-Krylov forces by integrating the pressure of each discretised panel. Although this method is still widely used as reference, nowadays, the solution neglects the effects of gravity, which limits the application to water entry process where the gravity can be not accounted . Sun and Faltinsen (2007) extended the method to include gravity, while Wu et al (2010) included the nonlinear velocity potential flow theory. Still, these methods do not

account for viscous effects and are still focused on the 2D cases or simple 3D geometries.

In the recent times, applications that aim to numerically solve the Navier-Stokes equations, known as Computational Fluid Dynamics (CFD) have becoming more used and developed. CFD has been widely applied to predict fluid behaviours and fluid-induced structural loads, motions, and deformations, in which the accuracy has been reported to be very good for analysing the hydrodynamic problem of interaction between a solid body and multi-phase flows containing free surface with viscous and turbulent flows well modelled.

In special, the open source CFD library OpenFOAM has been widely used in slamming problems. Wang and Guedes Soares (2020) have studied the effects of comprehensibility, three dimensionality and air cavity on a free-falling wedge cylinder, where the three scenarios are simulated using the Reynolds-Average Navier-Stokes (RANS) equations and volume of fluid (VOF) in OpenFOAM library and the results are compared to the available experimental data. Shen et al. (2016) used both OpenFOAM and star-CCM+ to simulate 2D sections and 3D models of a 10K container ship, where it stated that the dynamic overset grid technique in OpenFOAM had demonstrated its flexibility and efficiency for large amplitude motions, which is suitable for slamming problems (Shen, et al., 2016).

The process of verification involves figuring out whether a model implementation accurately depicts the implemented method and the model's solution. As a result, validation tests the solver's accuracy, while verification evaluates the solver's consistency (Wang, et al., 2022). The Correction Factor (Stern et al., 2001), the Factor of Safety (Celik et al., 2008), and the Least Square Fit approach (Eça and Hoekstra, 2014) are three of the most often used techniques to analyze grid and time step uncertainty. The Richardson extrapolation method forms the foundation of the first two approaches. The ITTC (2008, 2017) guidelines for uncertainty measurement in CFD studies recommend all of these methods.

As for the specific study of the pressure loads on a lifesaving boat, MARINTEK (Kauczynski, et al., 2009) has performed over 25,000 tests with 14 different lifeboats dropped from a skid or vertically. These tests were important specially to use as validation to the several numerical models and simulations eventually studied. Ringsberg et al (2017) presented a benchmark study with the aim to demonstrate the practical use of quasi-response methods for the assessment of impact loads on modern FFLBs, where eight different calculation methods were compared based on analytical plate strip models (linear and nonlinear idealizations), and FE models of different configuration and complexity (quasi-static linear, GNL, linear-elastic and transient dynamic). Qiu et al (2020) have established a mathematical model using the strip theory and Kane's method, where the FFLB motion is calculated from the beginning in the skid until the water entry, and after compared to the star-CCM+ simulation results. Huang et al (2021) have developed a model based on Computational Fluid Dynamics to holistically simulate and analyse the water entry process, applying overset mesh technique and not only comparing it with experimental data but also studying the influence of changing the dropping height and inclined angle.

The objective of the study is to simulate slamming problems in OpenFOAM, especially the entire process of the freefall of a lifeboat during its freefall and investigate the trajectory, pitch angle, velocity, acceleration, and pressures of the boat.

2 NUMERICAL METHOD

Open Fields Operation and Manipulation, also known as OpenFOAM, is a C++ toolbox for the development of customized numerical solvers, and pre-/post-processing utilities for the solution of continuum mechanics problems. For the purpose of this project, a multiphase simulation based on the VOF method is used. This method is relevant for engineering applications since it is applied when two immiscible fluids set the scenario studied (Manafpour & Hamzeh, 2017). Furthermore, this solver is applied over the chimera meshing technique so it can deal with large amplitude motion, which is the case of the majority slamming cases.

The tool from OpenFOAM that supports the VOF method and overset meshes is the overInterDyMFoam solver, which stands for overset and dynamic meshing version of interFoam. For two or more immiscible fluids, the VOF method is a surface-tracking method where the location of the fluid interface is of interest. The fluids in this model share a single set of momentum equations, and the volume fraction of each fluid in each computational cell is monitored over the entire domain. The physical formulation of this problem of two isothermal, incompressible and immiscible fluids is based on the continuity, momentum and interface capturing advection equations below, respectively (Albadawi, et al., 2013).

$$\frac{\partial \boldsymbol{\rho}}{\partial \mathbf{t}} + \boldsymbol{\nabla} \cdot (\boldsymbol{\rho V}) = \mathbf{0} \quad \textbf{(1)}$$

$$\frac{\partial (\boldsymbol{\rho V})}{\partial \boldsymbol{t}} + \boldsymbol{\nabla} \cdot (\boldsymbol{\rho VV}) = -\boldsymbol{\nabla P} + \boldsymbol{\nabla} \cdot \boldsymbol{\tau} + \boldsymbol{\rho g} + \boldsymbol{F_\sigma} \quad \textbf{(2)}$$

$$\frac{\partial \boldsymbol{\alpha}}{\partial \mathbf{t}} + \boldsymbol{\nabla} \cdot (\boldsymbol{\alpha V}) + \boldsymbol{\nabla} \cdot (\boldsymbol{V_C \alpha}(\mathbf{1} - \boldsymbol{\alpha})) = \mathbf{0} \quad \textbf{(3)}$$

where ρ is the fluid density, $\boldsymbol{V}$ is the fluid velocity vector, τ the viscous stress tensor defined as $\tau = 2\mu S = 2\mu(0.5[(\nabla \boldsymbol{V}) + (\nabla \boldsymbol{V})^T])$, μ the fluid dynamic viscosity, P the scalar pressure, $\boldsymbol{F_\sigma}$ the volumetric surface tension force, $\boldsymbol{g}$ the gravitational acceleration vector, $\nabla \cdot (\boldsymbol{V_C} \alpha(1-\alpha))$ an anti-diffusion heuristic term and α the interface capturing.

Regarding the floating body, it is modelled as a free rigid body where the forces considered are the gravity and the surface forces of pressure and shear stress (Benites-Munoz, et al., 2020). At each time step, the six DoF solver from OpenFOAM performs the integration of pressure and viscous stress component over the wetted surface S_H to assess the resultant force and moment around the CG. The accelerations are obtained by dividing both resultants to its respective inertia term and it can be integrated into velocity and displacement by the Newmark integration using $\gamma = 0.5$ and $\beta = 0.25$.

A general implementation for the use of unconnected (also known as Chimera) meshes is the overset framework in OpenFOAM. In this approach, two independent and disconnected meshes are created: the background and overset (chimera). This method is very helpful in situations involving mesh motion and interactions. It avoids the problems and instabilities associated with deforming meshes (Tisovska, 2019). The principle of this meshing approach is to give, at each time step, a label to each cell of both domains, where it describes if the cell is calculated, where the equations are solved for this cell; hole, where there is no computation for this cell; or interpolated, which is when the value is computed from the nearest elements of the other domain (background or overset).

Between the cells, there are the donors, which are the ones that provide values, and the acceptors, whose value gets set from interpolation. The simplest one and also fastest that is considered in this project is the "cellVolumeWeight", which uses weights proportional to the volume of the acceptor cell inside a given donor cell and normalized to the total volume of the acceptor.

3 A SLAMMING LOAD ON THE TWO-DIMENSIONAL WEDGE DURING WATER ENTRY

3.1 *Simulation setting*

The open-source CFD software OpenFOAM is used to perform simulations of the dropping wedge in two-dimensions. the overset (chimera) mesh approach is used here, which divides the discretization of the background domain, responsible for containing information regarding the fluids, and the overset mesh, for the solid body. The model considered for the study is two-dimensional and half of the scenario (wedge and background), simplified by using the boundary condition of symmetry patch. This consideration in important due to the considerable reduction of cells to be meshed, which also reduces the computational effort and time. With this, the general mesh with background, waterline and wedge is modelled as shown in Figure 1. Even though the simulation is two-dimensional, OpenFOAM performs as a three-dimensional extrusion, which in the case of this project was used a thickness of 0.01 m. What makes it a planar simulation is the empty boundary condition given to the front and back faces. As for the others, wall boundary condition was given to the right face and atmosphere standard boundary condition, as in Greenshields (2015) is given to the top face, while left is symmetry plane. Also, the water entry region has a denser mesh, since it is where all the events occur, and it is more important to be refined for better results. The refinement is shown in Figure 2.

The wedge is modelled based on the studies of Wang et al. (2015) at the centre left of the chimera mesh of dimensions 16 × 10 cm, where it starts with initial velocity above the water, wall boundary condition and 0.01 m of positive vertical offset is given for the simulation to not start with disturbed state. It is treated as rigid body constrained to move vertically only and, for this purpose, the 6 degrees of freedom OpenFOAM solver is applied to obtain the solution of the wedge's motion. The mass is also defined based on the 32.3 kg/m from Wang et al. (2015). The simulation's parameters are shown in Table 1.

Table 1 - Parameters of the wedge and simulation

Parameter	Value
Deadrise angle	30°
Mass	161.5 g
Initial velocity	2.5 m/s
Gravity	9.8065 m/s^2
Water density	998.2 kg/m^3
Water kinematic viscosity	1 mm^2/s
Air density	1 kg/m^3
Air kinematic viscosity	1.58 mm^2/2

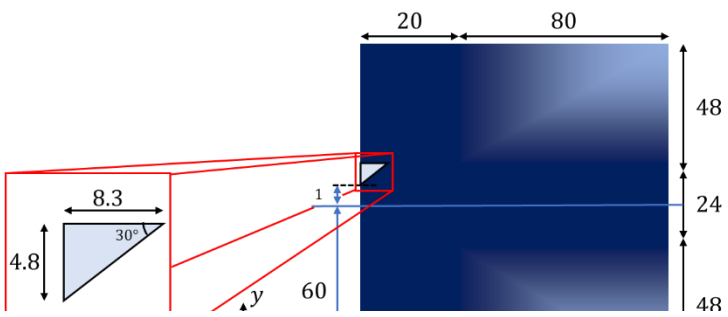

Figure 1 - Background mesh. Dimensions in cm and denser mesh over dark region

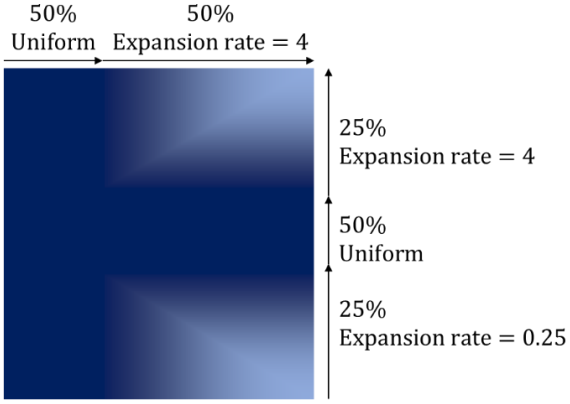

Figure 2 - Cell distribution along xy plane

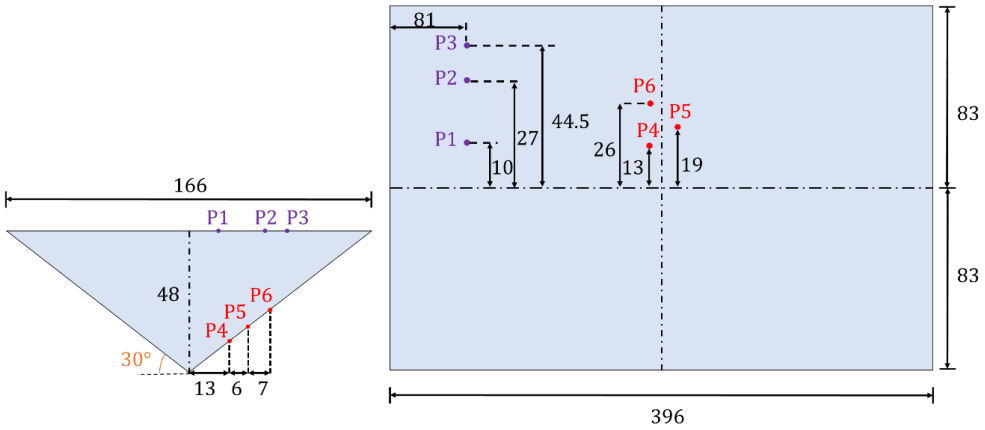

Figure 3 - Arrangement of the prismatic wedge and sensors from Wang et al. (2015). Units in mm.

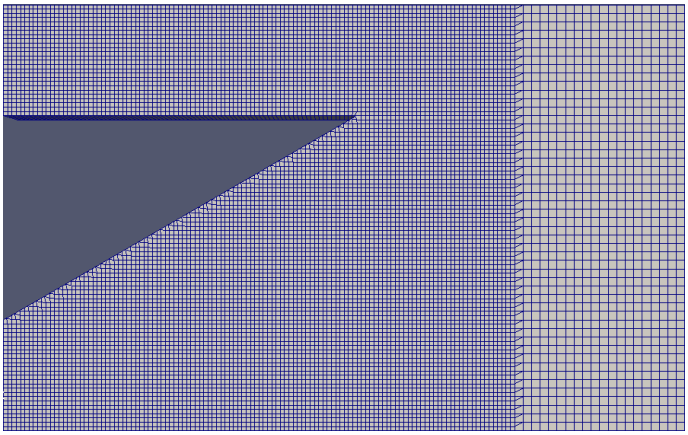

Figure 4 - Details on the medium overset meshing

Three simulations were performed with different mesh sizes and following the Figure 2 division. They are described by the smallest cell size in the water entry region, which are 4 mm (coarse), 2 mm (medium) and 1 mm (fine), defined also by a constant refinement ratio of 2. Pressure sensors (patchProbes) were set as in the experiments illustrated in Figure 3. The courant number was kept constant as 0.25 based on a timestep of 10^{-5} s. The overset mesh with the wedge was refined and extruded around the wedge, as shown in Figure 4.

The simulations were performed on a regular desktop equipped with an Intel Core i7-4570 @ 3.2 GHz with 94.1 GB of RAM memory and using 4 parallel simulations. Further details of the meshing and CPU time can be seen in Table 2. It is notable that the increase of the number of cells, the CPU is also more demanded by taking longer to process the whole simulation.

Table 2 - Meshing details and CPU time

	Minimum cell [mm]	CPU [h]	Background cells	Overset cells
Coarse	4	0.11	14,751	2,751
Medium	2	1.07	59,008	11,008
Fine	1	37.34	236,032	44,032

3.2 *Model validation*

The first results that can be used as parameter for validation are the pressure on the probes sensors input as described in Figure 3. For this comparison, two validation data are used, the experimental measurement, called as “experimental” in the next plots, and the two-fluid Boundary Element Method (BEM), called as “numerical”, both results obtained by Wang et al. (2015) studies. The CFD results by using three overset meshes setting are shown and compared in the Figure 5. The more refined is the mesh, the clearer the result gets, especially at the peak. This occurs due to the better-quality mesh, capable of better describing the continuous ambient as more discretized it gets. In general, the results are also in good agreement in the three approaches. The punctual differences that appear are the appear delay to the beginning of the ascension and the peak, which can be explained by the initial shift given to not disturb the background mesh in the simulation. Also, the peaks differ between each other due to the high uncertainties present in the experimental and numerical analysis, as concluded by Wang et al. (2021), which can also be noted on the large uncertainty bar presented in the results of Wang et al. (2015).

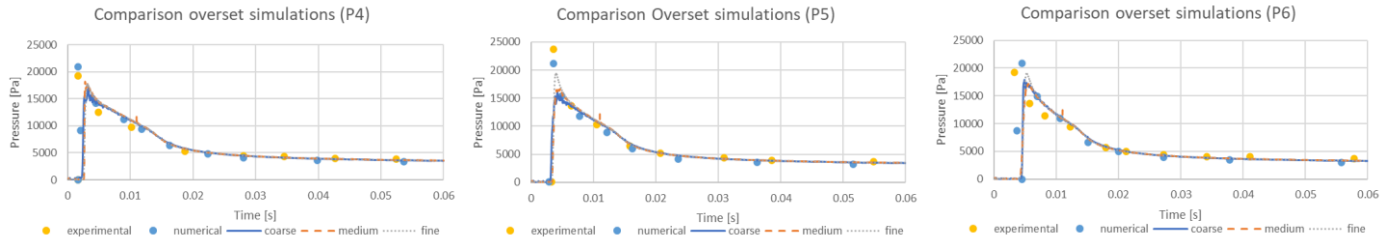

Figure 5 - Comparison of pressure results from CFD with different validation data from Wang et al. (2015)

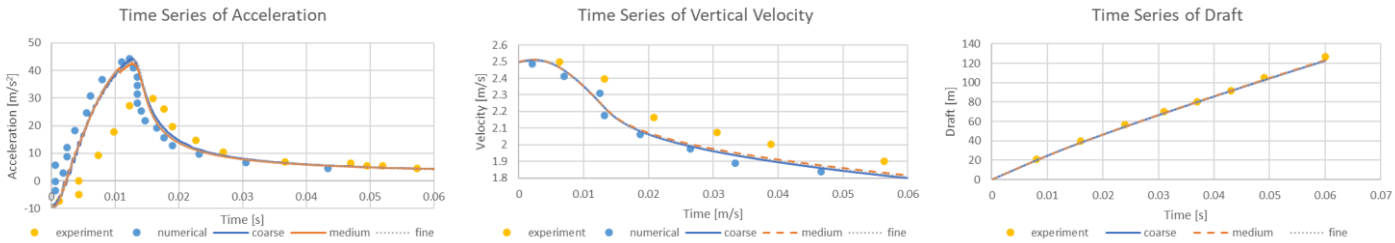

Figure 6 - Comparison between kinematics results from CFD with validation data from Wang et al. (2015)

What is also presented as result in the studies of Wang et al. (2015) is the kinematics of the wedge, including acceleration, velocity, and wedge draft, shown in Figure 6. In the draft time series, due to the high similarity of the experimental results and the numerical ones, just the experimental was considered. In all three cases, the 2D simulations are in better agreement with the numerical solutions, even considering the three different meshes. As for the difference concerning the experimental result and the numerical ones, the acceleration peak is notably higher, resulting also in differences of behaviour in the velocity time series. This has to do with three-dimensional effects neglected in the numerical methods, which was tested in Wang et al. (2021) by performing the same simulation but considering it three-dimensional and applying the actual length in a 3D domain. What is shown is that the acceleration peak reduces significantly near the experimental results, which means that this divergence is expected, and this model should agree better with the two-dimensional BEM numerical approach, which has few deviations due to potential flow consideration.

In order to perform the convergence research and quantify the discretization errors, the constant Courant-Friedrichs-Lewy (CFL) number is used, along with the approach of correction factor based on Richardson extrapolations based on ITTC (2008 and 2017) standards. The uncertainties associated can be assessed by a factor of safety approach (Roache, 2003), which can be used to define the uncertainty U_i with a factor of safety of $FS = 1.25$ for careful grid studies to bound simulation error. The factor of safety strategy, albeit not suggested by Roache (2003), can be employed in circumstances when the answer is corrected with an error estimate from RE and also calculate a corrected uncertainty, U_{ic}. With this, the maximum acceleration and maximum slamming pressure coefficient, $C_p = p(t)/[0.5\rho V^2(t)]$, where $p(t)$ and $V(t)$ are the instantaneous pressure and velocity, and ρ is the water density, are analysed by this method, and the summary is shown in Table 3.

3.3 *Comparison with deforming mesh method*

The same scenarios were investigated in Wang et al. (2021), but instead of chimera meshes, the researchers applied the morphing mesh using the same software for reducing computational expenses. The simulations from this investigation were recreated using parallelization to reduce the computational time. A

Table 3 - Uncertainty calculation for maximum acceleration and pressure coefficient

Uncertainty calculation		Maximum acceleration [m/s²]	Maximum C_p
Output values	$Ø_1$ (fine)	43.77	6.801
	$Ø_2$ (mid)	42.66	6.925
	$Ø_3$ (coarse)	44.41	5.948
Refinement ratio	r	2.00	2.00
Convergence ratio	$\epsilon_{21}/\epsilon_{32}$	-0.6345	-0.1275
Order of accuracy	p	0.6564	2.9709
Approximate relative error	e^{21}_a	0.0254	-0.0183
	e^{32}_a	-0.0410	0.1411
Extrapolated relative error	e^{21}_{ext}	-0.0422	0.0027
	e^{32}_{ext}	0.0767	-0.0202
Grid convergence index (GCI)	GCI^{21}_{fine}	2.80E-05	0.011
	GCI^{32}_{fine}	9.27E-05	0.018
Uncertainty	U_1	0.014%	0.335%
	U_2	0.046%	2.578%
Corrected Uncertainty	U_{1c}	0.003%	0.067%
	U_{2c}	0.009%	0.516%

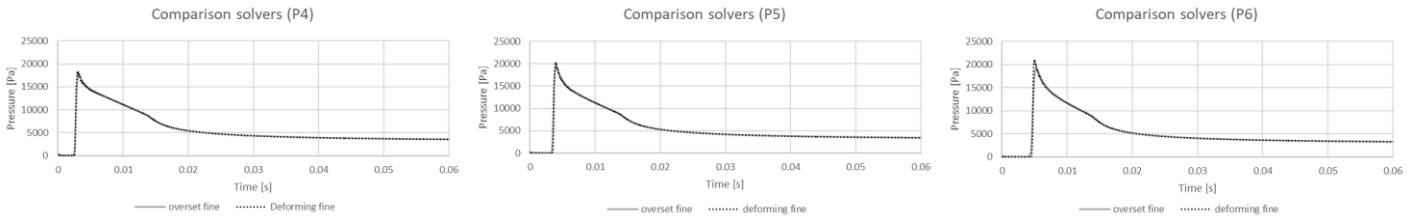

Figure 7 - Pressure comparison between fine deforming and overset meshes

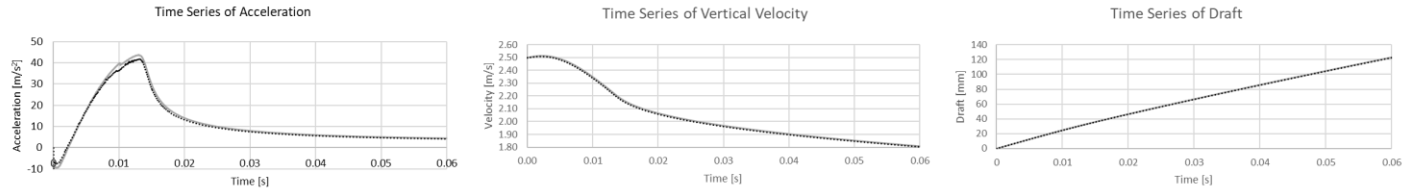

Figure 8 - Comparison between kinematics of the wedge for deforming and overset meshes

comparison between computational time of using chimera and deforming meshes using similar mesh size and parallel processors is shown in Table 4. What is already seen is that the overset mesh method requires more of the CPU than the morphing method, even by using 4 parallel processors to run the simulations. This happens mostly due to the drawback of additional computational load introduced by the interpolation process between domains (Berton, et al., 2017).

Table 4 - Comparison between CPU time, in hours

	Deforming	Overset	Difference
Coarse	0.035	0.11	214%
Medium	0.462	1.07	132%
Fine	4.896	37.34	663%

Comparisons are made between the dynamic and kinematic results of the wedge water entry problem. The first is the pressure from the sensors P4, P5 and P6, as shown in Figure 7, by considering the finest mesh of both methods. In general, the results are in accordance with each other, and differences are observed mostly at the peaks. While for P4 and P5 this difference remained at 3.4% and 4.4%, respectively, for P6 this was more discrepant, with about 10% difference. These regions are known to variate to a great extent for how refined the mesh and time step are, and the difference between resolutions observed in the comparison between contour plot in Figure 9 and also, in the results related to dynamics, such as acceleration – as a result from force integration – and pressures, can be an explanation for that together with the convergence velocity, which tends to be faster for overset mesh approach (Lopez Mejia, et al., 2021). As for the kinematics ones, which the comparisons are shown in the plots of Figure 8. There are differences of 4.2% between the peaks of acceleration, but mostly show the same results. This variation is even less perceptible in the velocity and penetration results shown in Figure 8.

4 LIFEBOAT CFD SIMULATIONS

4.1 *Simulations setting*

To evaluate the possibility of performing the loads assessment and the vessel's motion prediction, a case study is done by using a model of lifeboat and a simpler scenario of how its free-fall would occur by neglecting the initial velocity and spin given by the skid, starting from rest at an initial dropping height H and angle α. This model is a recreation based on the Schat Harding 1000, typically used by researchers (Ringsberg et al., 2017; Huang, et al., 2021) to compare the assessments with the experimental study made on the full-scale model (Kauczynski, et al., 2009). For this project, however, it was not possible to use the exact same model due to copyright matters.

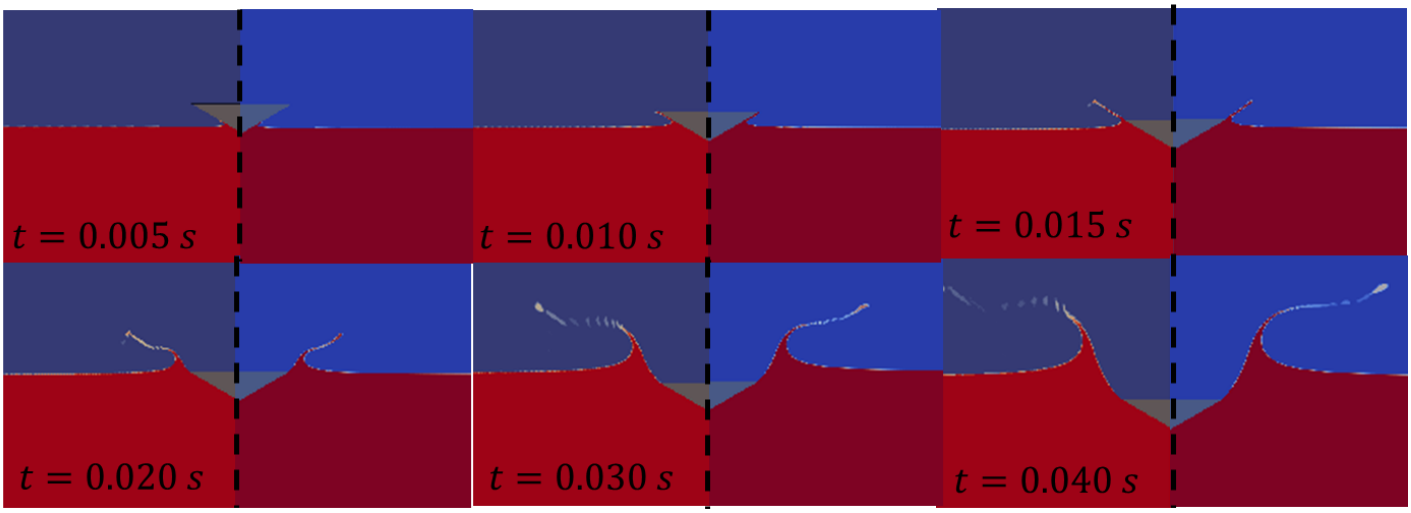

Figure 9 - Contour plot of alpha.water over time for fine deforming (left) and overset (right) meshes

Even so, the geometry could be reproduced by using the body plan from Figure 10 and the side view of the ship in Rhinoceros from Figure 11 The lifeboat's main particulars are also shown in Table 5. The result of this reproduction is shown in Figure 12. Distortions of shape and dimensions of about 5.4% have occurred in the process.

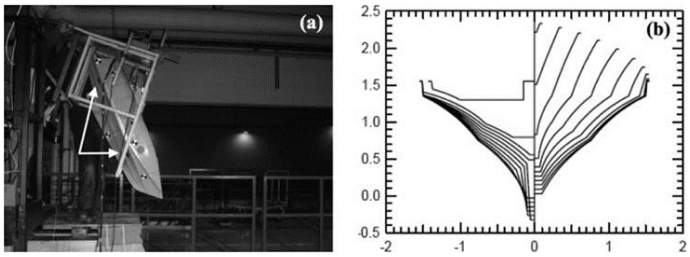

Figure 10 - (a) Lifeboat skid setup; (b) Lifeboat's body plan (Ringsberg, et al., 2017)

Table 5 - Main particulars of the full-scale lifeboat (Ringsberg, et al., 2017)

Parameter	Value
Overall length [m]	12.57
Overall width [m]	3.34
Displacement [ton]	16.8
LCG forward of stern [m]	5.29
Radius of gyration in pitch [% of L_{OA}]	25%

The domain and mesh are set with similar philosophy from section 3.1 with the major difference of being a 3D simulation, as illustrated in Figure 13, and instead of empty patches, there is going to be two more walls on the front and back. The overset domain dimensions are shown in Figure 14, and it has the same Dropping heights of 10 m, 20 m and 30 m are simulated with falling angles of 10° to 70° with 10° step, totalizing 21 simulations. The scenario, axis convention and the cell concentration division are illustrated in Figure 13. The origin is set to be on the waterline with coordinates (x, y) equal to the centre of gravity, and the cells are chosen to have about 40 cm in the water entry region and chimera. The division and distribution of the cells also follows what is proposed in Figure 2, but also considering the other side of the symmetric plan (which means the proportion in each axis is 25%, 50% 25%). The physical constants are also the same from Table 1. Although this situation would end in a turbulent flow, the simulation is set as laminar to use a more stable solver with less crashing chances.

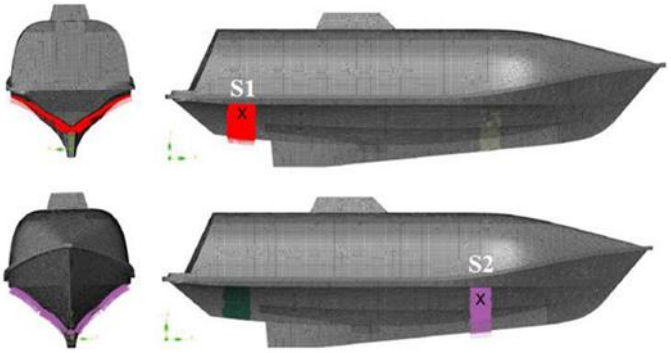

Figure 11 - Front and sideview of the lifeboat (Ringsberg, et al., 2017)

The time step used was 10^{-3} s, and to capture sufficient details for a water entry problem, the Courant number is set to be always smaller than 0.3 based on the analyses of Muzaferija (1999). 5 seconds of journey, starting from the beginning of the freefall.

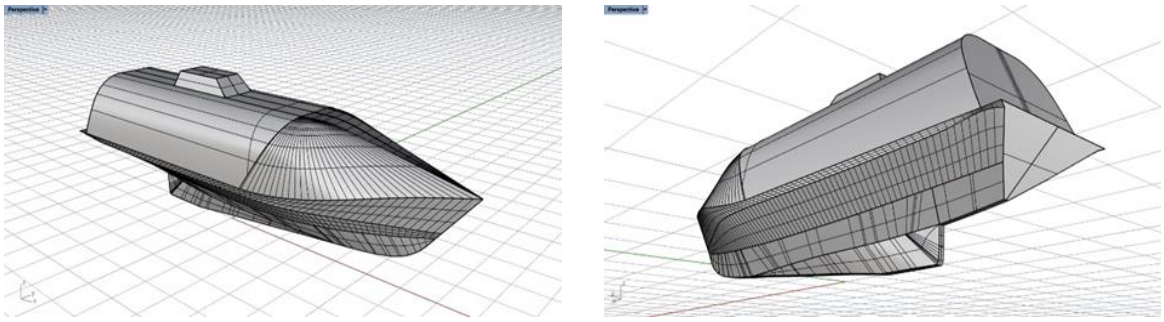

Figure 12 - Reproduction of the lifeboat hull surface in Rhinoceros

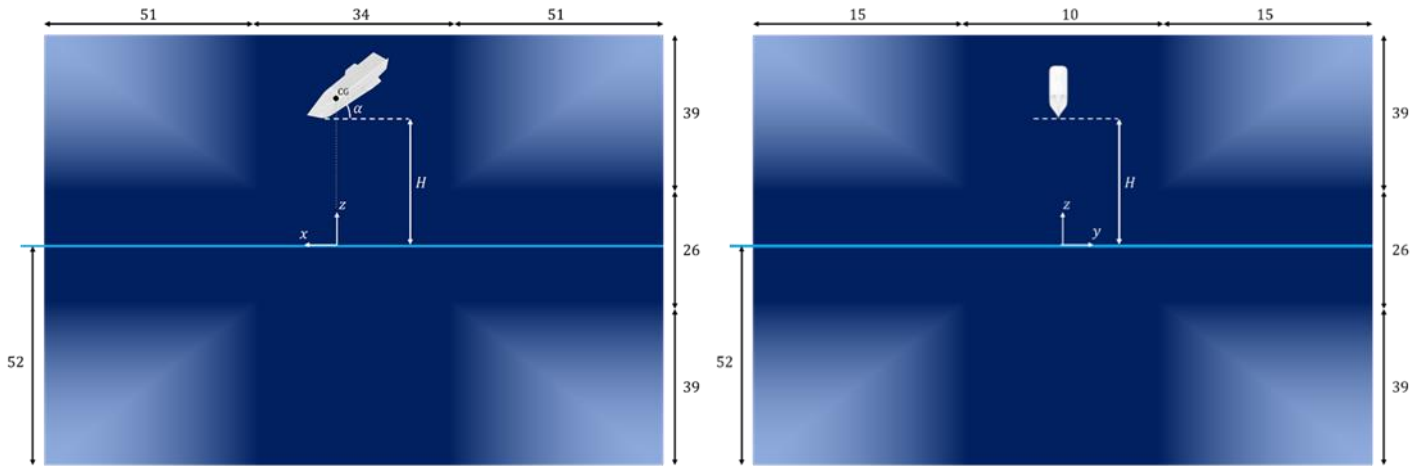

Figure 13 - Views of the background domain for de lifeboat. Dimensions in meters

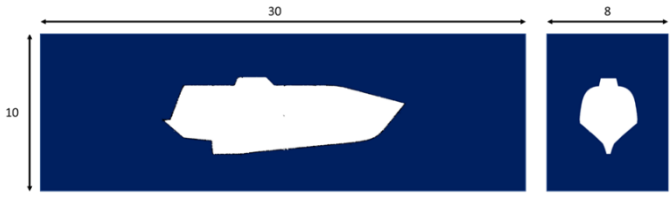

Figure 14 - Dimensions of overset domain in meters

4.2 *Preliminary analysis*

An overview of the general simulation is done with comments and considerations on it. Regarding the mesh and computational effort, an Intel Core i9-4570 @ 3.2 GHz with 126 GB of RAM memory was used, and since these simulations are expected to demand a lot more than the wedge did, they were parallelized into 27 processors. The general overview of the simulations' parameters is shown in Table 6. Even though the simulation time was reasonable, this was just possible by using almost 7 times more parallel processors and also using a mesh less refined with a larger minimum cell size. This is expected due to the increment of one dimension in the simulations and also in the motion of the body, increasing the complexity of the calculations for an overset approach.

Table 6 - Summary of the lifeboat`s simulations components

Parameter	Value
Background cells	1,141,292
Overset cells	36,292
Minimum cells [cm]	40
Time [h]	About 4 h

What also influences this is the meshing. In the case of the overset, which has the snapping process, the result can be seen in Figure 15. The process resulted in a shape similar to the designed lifeboat but with some deviations due to the snapping process. This alteration is expected for coarse meshes where the refinement of the snapping process is not enough to acquire all the information, which was the result of a choice to have faster and more stable simulations where the whole lifeboat journey can be described. Since the geometry is based but not the same as the Schat Harding 1000 used in the experiments, the time of simulation was prioritized over the mesh refinement even for checking how the results and the lifeboat in general behaves.

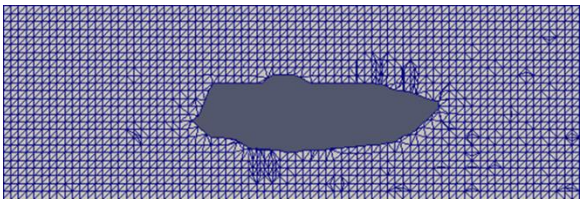

Figure 15 - Sideview of the overset mesh with the lifeboat external surface

By being modelled over the Schat Harding 1000, even if slightly different between each other, the model can still be checked on the pressure sensors used in the experiments of Kauczynski, et al., 2009 by at least seeing how it behaves. The results are shown in Figure 17. What is first noted when comparing the results is that the numerical values does not match, which was expected due to the changes on geometry, mesh, and turbulence model. Qualitatively, the behaviour match between each other, with differences on how fast the peak grows and decay. This has to do with how both pressures are measured, while one uses a plate sensor that measures the average force over a surface with larger area which makes the peak decays faster, while the computational cell is infinitively small (Huang, et al., 2020). This means that, physically, OpenFOAM can assess and give great contributions, and qualitatively, it would require more refinement and time to simulate each case.

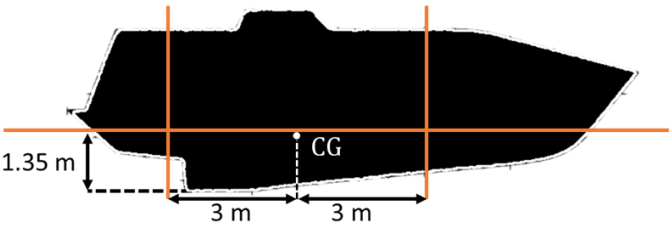

Figure 16 - Planes for pressure study

4.3 *c*

After the preliminary analysis, the study can be extended to do an overview of the pressure over the hull. In order to do this, the pressures on the intersection between the hull and three planes are considered as shown in Figure 16. The transversal planes in bow and stern are divided into 11 points over impact surface (hull below) where the pressures are taken, while for the longitudinal plane, 21 points are considered, as shown in Figure 18.

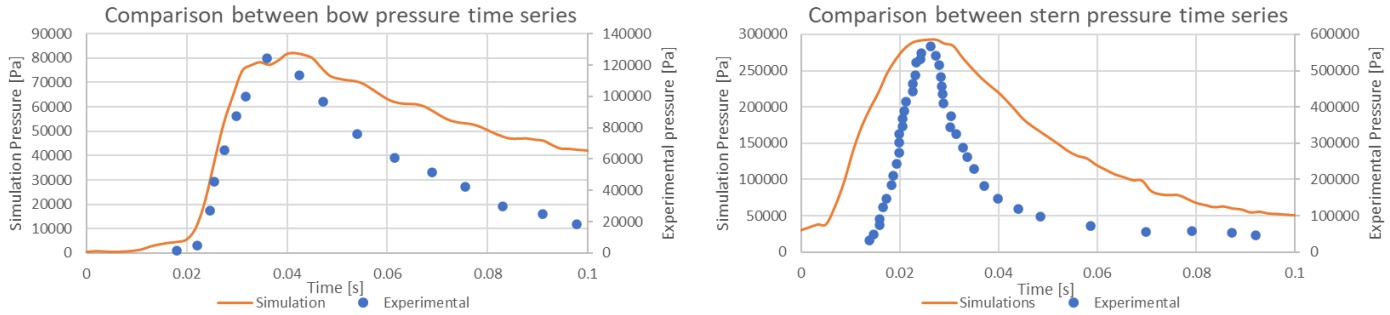

Figure 17 - Bow and stern pressures compared between CFD results and experimental measurements

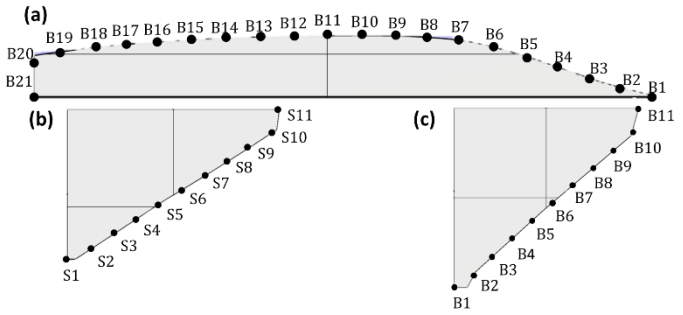

Figure 18 - Probes sensors on (a) longitudinal plane; (b) stern plane; (c) bow plane

Regarding the pressures on the stern plan for the same height and different angles, as in ,in general, they all present the same behaviour with different peak values, mostly. Some simulations results are the same due to the space between control points being not enough to be in different cells with different properties and parameters. The highest peak is the 3 lowest points on the keel, while the highest one at S11 has negative pressure due to the water jet detachment at this point, and in general, the higher the point, the lower the pressure will be, except in 50° where S5, S6 and S7 were lower than S4. The angle with highest pressure was 50°, which already can indicate which scenario would have larger impact loads.

The same analysis can be performed for the selected bow plane, as in Figure 20. They are considerably lower than the stern entry, indicating what the rotation during water entry can provoke another slamming itself on the back of the hull. They have different shape even if they have peaks, especially in the case of 70° compared to the rest. This can be explained on how the boat entries the water as shown in Figure 30. As for the behaviours, similarly the bottom control points are usually the highest peak, where the first two competes for the highest, while the less critical was the highest one on the boat due to the water detachment. It is results with larger peak bells and by being a demanded region, especially in what concerns forward velocity.

Regarding the assessment for the longitudinal planes, the summarized results are shown in Figure 21. Usually there are two highlighted peaks, one for L1, which means the forward border, and another one for the other in the middle before ending the simulation, except for the 10° launch, which also has to do with the way the boat dives. What is also notable is that the one with higher peak is also from 50°

In Figure 22 the comparison is not between angles, but dropping heights, and all abscises were set to start at the free-fall time, which is $t = \sqrt{2H/g}$. The B sensor is referred to B2, while S stands for S3. It is notable that the behaviour of the pressure curves is mostly the same for different heights, with the difference on the pressure peak, which is strongly influenced by the gained velocity from freefall. They differ not only by the peak value on top, but also in the decay velocity, which becomes faster for the higher it starts from. The peaks also get closer to each other for greater heights due to this same relation: the faster velocity that the

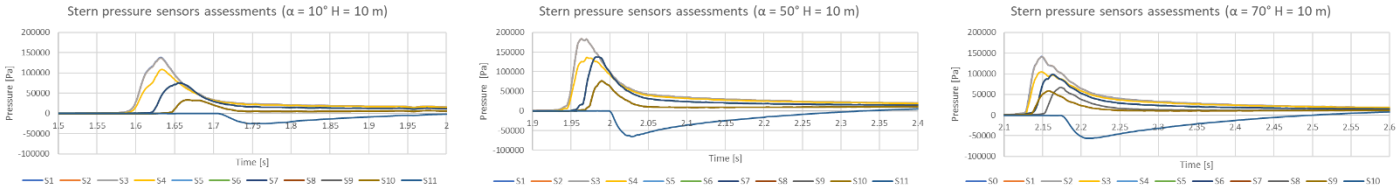

Figure 19 - Time series of stern pressures for dropping height of 10 m

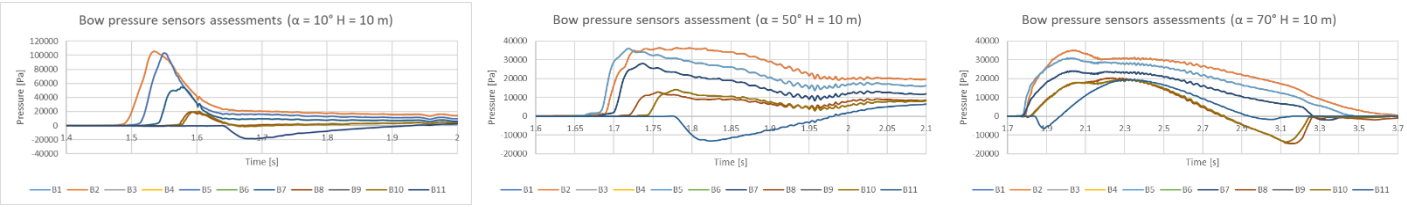

Figure 20 - Time series of bow pressures for dropping height of 10 m

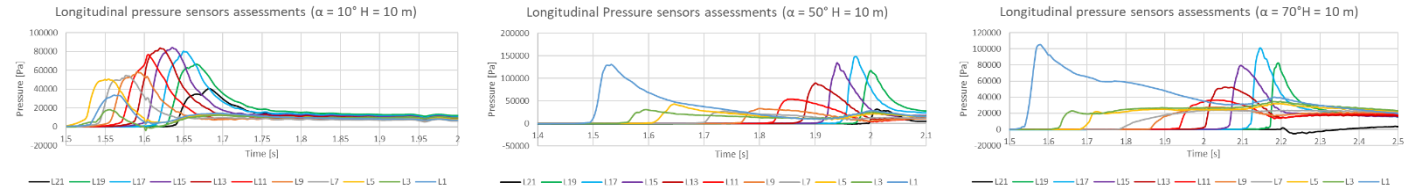

Figure 21 - Time series of longitudinal pressures for dropping height of 10 m

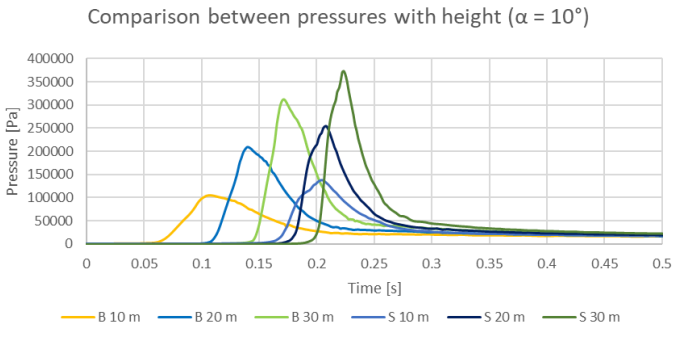

Figure 22 - Comparison of pressure for different heights and α = 10°

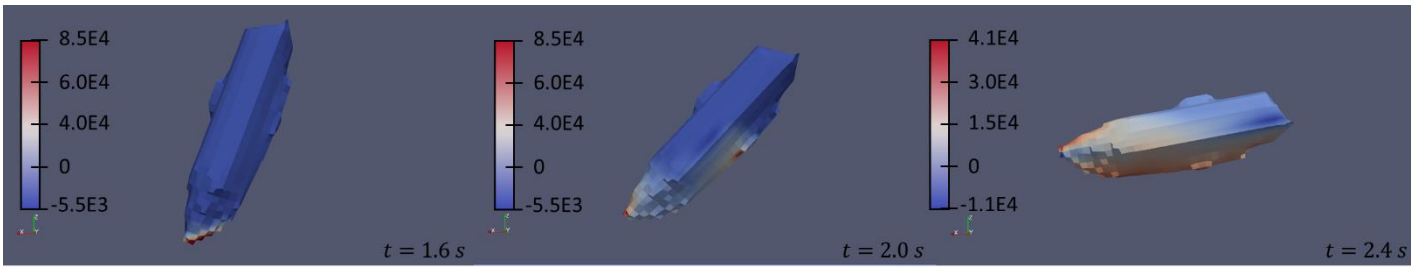

Figure 23 - Pressure contour plot for α = 70°. Units in Pa

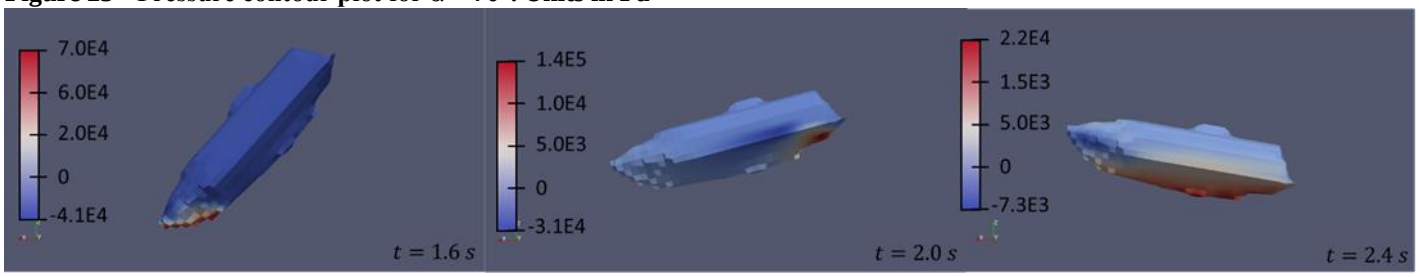

Figure 24 - Pressure contour plot for α = 50°. Units in Pa

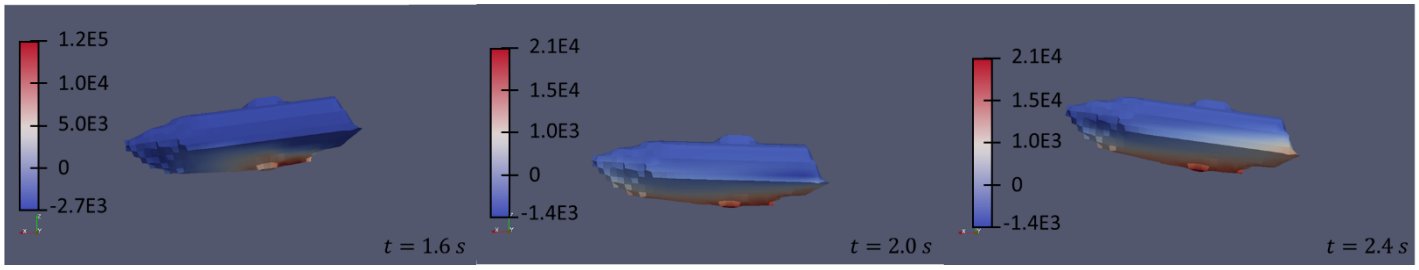

Figure 25 - Pressure contour plot for α = 10°. Units in Pa

lifeboat acquire reduces the time which the event occurs.

When using probes, it is possible to see how the pressure behaves along time in a specific point, but it is not possible to analyse what happens to the whole surface. Figure 23 to Figure 25 shows the contour plots of the pressure for 10°, 50° and 70°, starting from 1.6 s when the lifeboat starts entering the water. It is limited to the output interval previously defined and also on the memory of the computer used, but it has the advantage of mapping the pressure over the whole surface and even indicate where the pressure sensors should be input in the next simulation. The first two time instants considered are the most critical for the lifeboat, where the highest peaks appear due to the water entry. After this the pressures decays until further stabilization at a lower value. What is noticeable in all simulations is that the keel is the boat element where the pressure peaks concentrate, which is expected since there is the impact region with the water at high speed.

Two regions are of interest where the peak loads concentrates: the bow deck and the stern. The bow is the first to enter and receive the highest loads due to the impact with calm waters. After this, the turnback that the ship suffers due to the restorative moment given by the water buoyancy makes the stern also hits the water, creating another slamming impact, and one with ever higher peaks than the bow. This just not happens with the 70° scenario because in this case, the lifeboat dives before getting this turnback rotation, and the peak for diving is lower than for hitting.

4.4 *Kinematics analysis*

In this part, the general kinematics of each simulation is discussed. The simulations have planar motion instead of unidirectional as it was with the wedges in chapter 3. This kind of assessment also has importance besides the impact loads due to the importance of how the lifeboat will respond when it is required in an emergency. In general, it should get as far away as possible from the hazardous event when launched, and also its journey should not harm or injure the people on board.

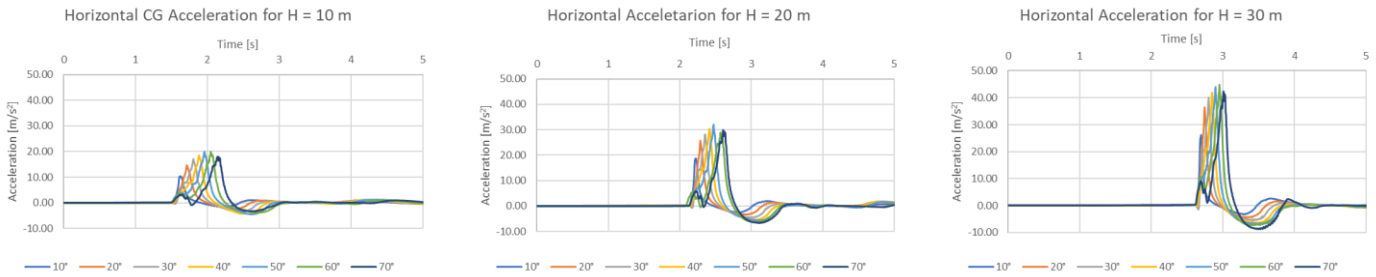

Figure 26 - Lifeboat's horizontal acceleration time series

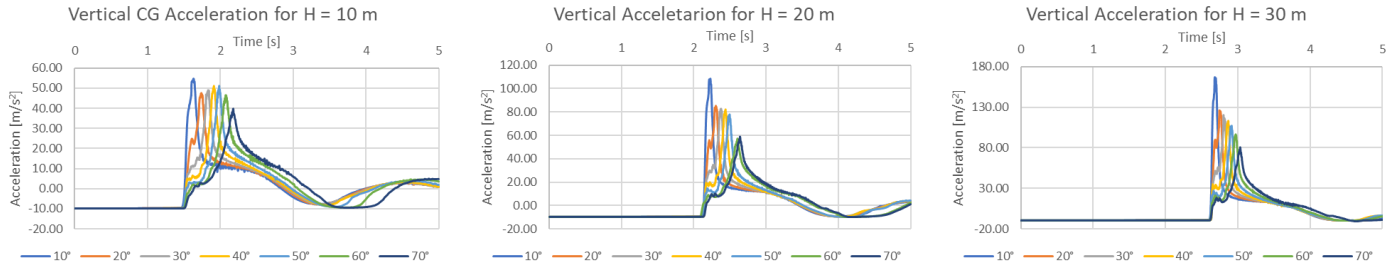

Figure 27 - Lifeboat's vertical acceleration time series

Firstly, what can be analysed is the acceleration in each direction in Figure 26. The horizontal acceleration in this kind of study is important because it is what gives the initial velocity that makes the vessel move forward from the dangerous zone. What is first noted is that the higher the dropping height is, the higher the acceleration gets. The peaks can give an idea of which cases the boats would not go far, being the ones with smallest peak due to the fact that they would not acquire much initial horizontal velocity. Similarly, this analysis can be extended to the vertical acceleration, shown in Figure 27. The behaviour was similar to what is seen for the horizontal acceleration, there is a positive peak before a negative one, expected for floating dynamic structures. The peaks seem to be larger, which has most to do on how long it takes to override and invert the vertical velocity and how was the trajectory on the water. The free-fall stage is marked by the constant acceleration of g for vertical acceleration and close to 0 for horizontal. Also, regarding the dropping heights, what is remarkable is that the greater the height, the greater is the acceleration peak, which is expected because the highest the boat fall, the highest is the velocity before hitting the water that should be nullified.

The acceleration is an important factor to consider when dealing with watercrafts, lifeboats especially, because exaggerated acceleration can increase the probability of injuries on board, and depending on the acceleration intensity, it can be even fatal to humans (Pearce, 2020). One way to assess if the case's accelerations are adequate is to use the IMO Combined Acceleration Response (CAR), shown in (Netherlands Regulatory Framework - Maritime, 1993), where the Square Root Sum of the Squares (SRSS) acceleration should not surpass the ellipsoid with axis of 15 g's in the +/- x axis and 7 g's in another axis, as shown in Equation (4).

$$CAR_i = \sqrt{\left(\frac{a_{x_i}}{15g}\right)^2 + \left(\frac{a_{y_i}}{7g}\right)^2 + \left(\frac{a_{z_i}}{7g}\right)^2} \leq 1 \quad (4)$$

To assess which cases simulated could be dangerous for people, the seats are assumed 90° and front facing. Additional centripetal and tangential accelerations due to rotation are neglected, which is reasonable for small crafts and for this case which the chairs angles and positions is unknown. In this case, the conversion of acceleration from the global cartesian coordinates to the seat relative's coordinate can be done by rotation matrix transformation. Table 7 contains the results for maximum CAR obtained with these premises. What is seen is that for greater heights and lower angles, the acceleration can be problematic and risky for the fleeing crew and passengers. This does not mean that people will get injures in these other cases, but the probability of human injuries is greater (IMO, 1991).

Table 7 - Maximum CAR for each simulation

	10°	20°	30°	40°	50°	60°	70°
10 m	0.81	0.72	0.74	0.78	0.79	0.73	0.63
20 m	1.60	1.29	1.25	1.25	1.21	0.92	0.96
30 m	2.45	1.90	1.84	1.73	1.73	1.53	1.31

Another kinematic parameter that can be analysed is the velocity. This measure has less to do with how smooth or hard will the lifeboat enter the water, but more related to how the kinetic energy gained with the free-fall is converted. Ideally, the falling velocity should be turned integrally into forward velocity, but this is not what happens, since there is loss of energy to waves, viscosity and even for heave oscillating. The horizontal velocity plots are shown in Figure 28. In these plots, a peak followed by a positive forward velocity with some variations is observed. As it was analysed before, the lifeboats with smaller horizontal acceleration peak ended up with smaller peak velocity

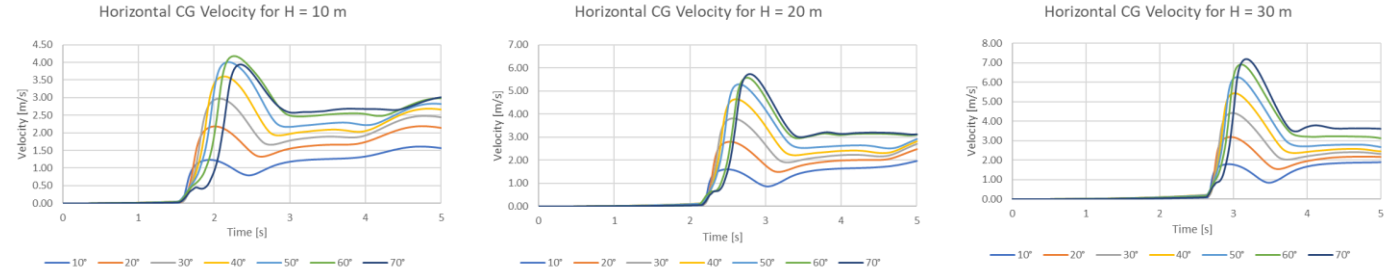

Figure 28 - Lifeboat's centre of mass horizontal velocity time series

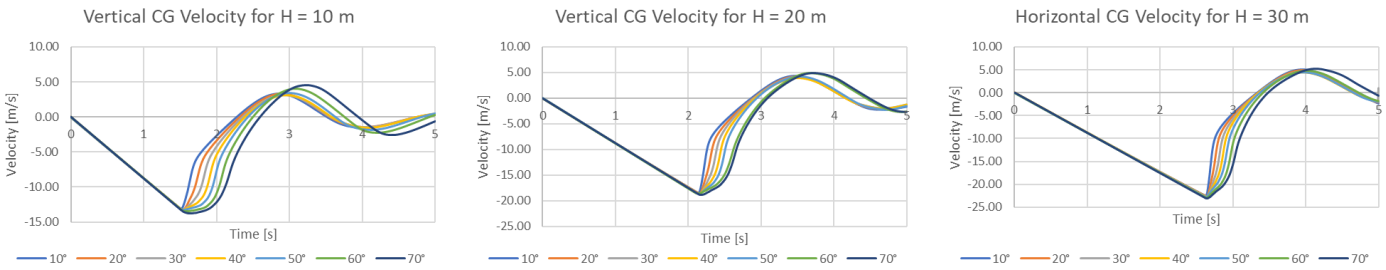

Figure 29 - Lifeboat's centre of mass vertical velocity time series

and stabilized at an inferior velocity, not being appropriate to flee from a hazardous event, while the ones with greater peak disputes the highest velocity depending on the angle and height. In this case, 60° has shown to be more efficient for lower heights, while 70°, for higher. As for the vertical velocity, shown in Figure 29, the initial tendency is linear with constant rate of g, as seen before with the acceleration, and after the free-fall stage, it oscillates around zero, which the tendency would be to continue until this dissipates into waves, mostly. What is also remarkable is that even with different initial velocities, the first positive peak right after entering the water was close to 5 m/s or below it.

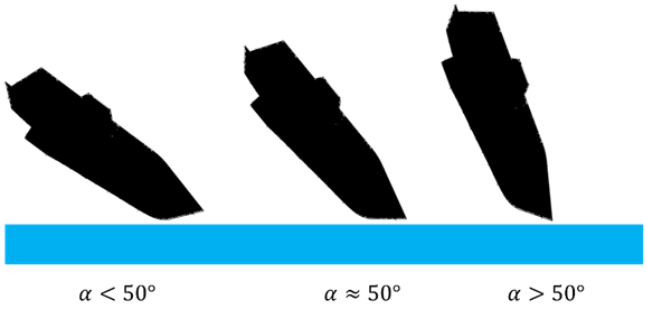

Figure 30 - Possible lifeboat entry depending on the angle

One aspect to notice not only in the velocities' plots, but also slightly in accelerations that 60° and 70° had a distinct behaviour compared to the rest, not as an outlier from the rest, but because their water entry occurs differently from the others. The reason is due to the lowest point that enters first the fluid, where for angles below 50°, approximately, the bow part of the keel is the first to touch, while for the ones above this angle, it the bow deck, which is illustrated Figure 30. The slope's change of the keel curvature changes how the boat is pushed and even suffers from a brake right when the slope changes. This explains why the horizontal acceleration has two peaks and why their velocities peaks are a little delayed.

It is possible to integrate the velocity on time and obtain the offset from the initial position. This shows effectively which scenario, in a 5 second interval, would go further when dropped from a certain height, as shown in Figure 31. In this interval, the best ones that could go further were the 60°, for smaller height, and 70°, for bigger. If the interval was smaller, the other boats would be more suitable due to the delay on the velocity peak caused by the angle of water entry, but even so, the higher peak and stabilization on a higher velocity makes them displace further. As for the vertical offset, it presented what was expected from the vertical velocity part. Initially, during the free-fall stage, the time series is parabolic due to the constant gravity and when entering the water, the boat starts to freely oscillate with reducing amplitude due to loss of energy.

Since all simulations were performed to have 5 seconds, it is possible to notice at what point the lifeboat is when $t = 5\ s$ which is when its trajectory is "interrupted". Besides the stabilization that the ship starts by damped oscillations after water entry, the greater angles have longer firs valley when entering the water, which is due to the pitch rotation that the vessel suffers to reach the equilibrium angle after a large amplitude is given. This also has to do with the submergence that the ship goes through in these particular high angles. the changes on the trajectory with different heights did not bring considerable differences as did the other parameters, except for the diving part or the number of oscillations. From one point of view, this can mean that changing the height did not bring much faster response to leave the hazardous event. On the other hand, the analysis would be different if the free-falling time was not considered. If removed and just considering the water entry part, these 5 s simulations turn into 2.38 s limited by the 30 m drop height case, and the difference of treatment can be seen in Figure 32.

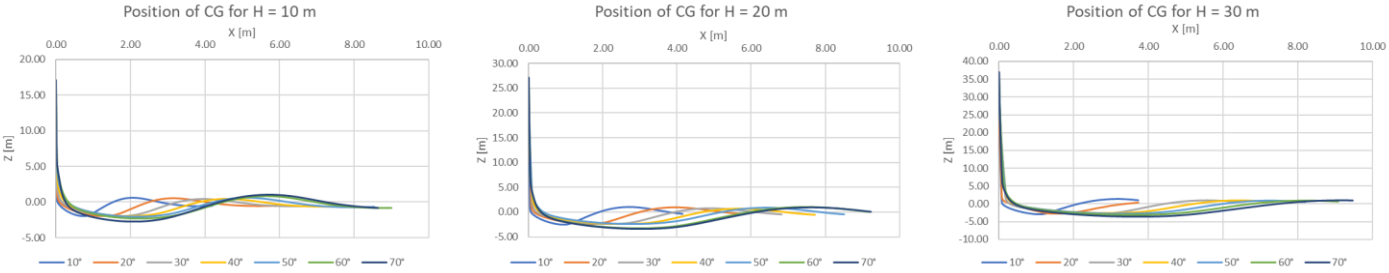

Figure 31 - Centre of gravity trajectory over time

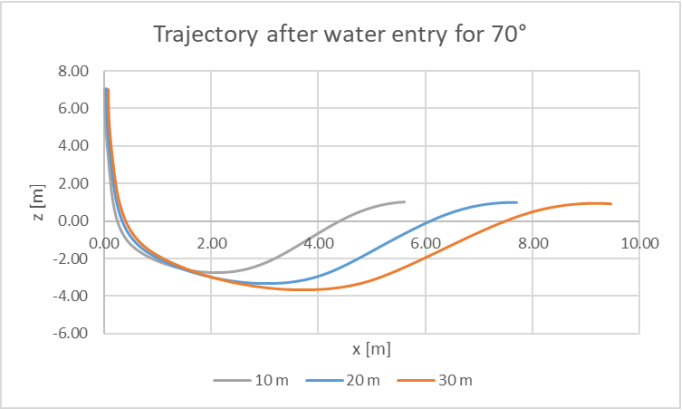

Figure 32 - Position of CG during water entry with α = 70°

The information of the CG position over time and pitch motion can tell how the motion of the lifeboat along its whole journey was. More than that, OpenFOAM stores the parameter α of the whole domain for each time step set for output. This mapping can also be plot using paraView, in special by removing the cells considered holes and slicing in the middle of the longitudinal plan. The results of this simulation can be seen in Figure to Figure 35 where just the angles 10°, 50° and 70° were plot and displayed. Comparing the water entry of the presented situations, it is notable how the increment of the angle makes the lifeboat more likely to submerge, as seen in Figure 33 to Figure 35, where the lifeboat dives closer to the free surface, while for 70°, in Figure , the boat already enters almost completely under the water, which did not occur because it did not have enough velocity to it. For the first two angles, mostly just the under hull had hit the water, making the keel absorb most of the impact and converting less energy into actual motion for the lifeboat.

5 CONCLUSION

The slamming phenomenon has still been a long-lasting topic for naval industry and engineering. Many methods can be used to assess the loads of this phenomenon, and the selected one for lifeboats was using the VOF method combined with overset mesh techinique in OpenFOAM.

For a first approach with this methodology, simple two-dimensional simulations of the water entry of a 30° wedge were carried out. The scenario was fully based on the experimental investigation executed by Wang et al. (2015), together with the BEM method, also calculated by the researchers. Three simulations were performed with a constant refinement ratio of 2 for later perform uncertainty analysis. Pressure could be compared, and, in general, they presented good adherence with the BEM and experimental results, especially after the peak, which was the part that presented higher divergence.

As for the kinematics parameters, the adherence was better with the BEM method results, while a higher discrepancy was observed between these both results and the experimental one. This is expected due to the three-dimensional nature of the experiment, while the models are both two-dimensional. The convergence of the parameter's maximum acceleration and pressure coefficient was also examined using the constant CFL method to perform uncertainty analysis. Both presented oscillatory convergence and uncertainty fall below 5% and even below 1%, when adding correction factors. Comparisons between morphing and overset mesh were also done and mostly the results were the same and differences can be spotted at peaks of pressure, which is usually more conservative for deforming mesh, and in the resolution of the results, which has shown to be better for overset mesh, which happens due to the structured and undeformed background and near-body. Even though, the computational time for morphing mesh was fairly lower than chimera, so in this scenario where the motion amplitude does not crash the simulation, both presented to be robust methods to assess this problem

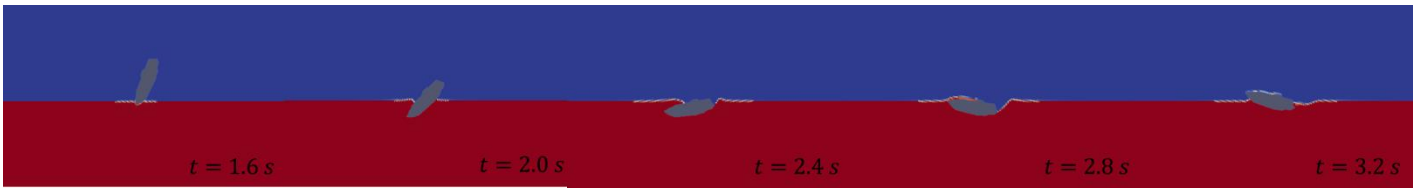

Figure 33 - Contour plot of alpha.water for 70° angle

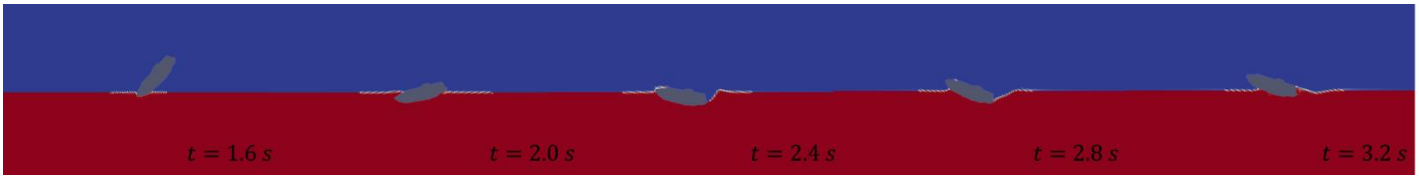

Figure 34 - Contour plot of alpha.water for 50° angle

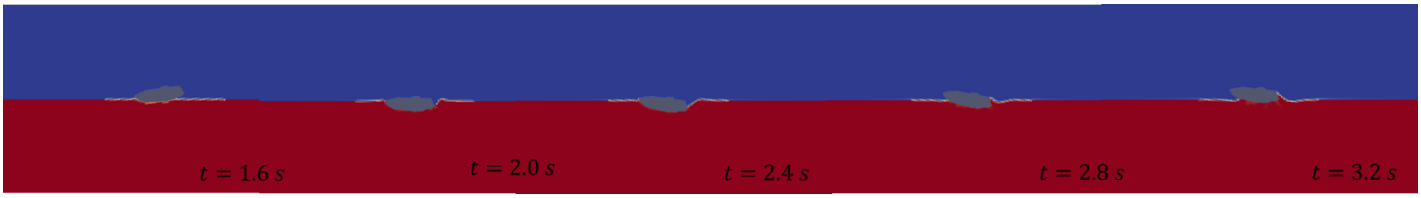

Figure 35 - Contour plot of alpha.water for 10° angle

and can be used to examine other hydrodynamic impact issues and model wedges of various forms.

Later on, simulations of a freefall lifeboat were carried in order to assess impact loads, predict how the lifeboat will behave when launcher with a certain angle and dropping height and also to evaluate if OpenFOAM can be a good tool for this type of analysis. The lifeboat model needed to be defined, and the simulation's inputs needed to be set. Using the data from the literature, a geometry based on the Schat Harding 1000 was modelled with simplified chines and distortions to the original dimensions of roughly 5.4%. The model is nevertheless based on a genuine lifeboat and has appropriate characteristics for our purpose. The simulations demonstrated to have a higher complexity compared to the wedge simulation, which is something to expect when dealing with the three-dimensional simulations. Discrepancies between the pressure values were found when comparing to the Marintek experimental measurements due these reasons and also the differences of nature to obtain this result.

Following this, a number of simulations were run for various descending angles and heights and then compared. The parameters pressure, acceleration and velocity typically tend to rise with the increment in height, which is to be expected. The displacement depends on considering just the water entry process or the whole journey with the freefall part, in which the first tends to be fairly different while the other does not present considerable differences. In terms of pressures, the peaks are typically focused in two areas: the bow deck, where the boat first enters the water, and the stern, where it enters the water again. With the exception of the 70° case, where the boat's submersion softened the peak, this stern peak is typically higher than the bow. The kinematics was used to also assess how harmful can be the freefall and the water entry process for people by assessing accelerations. It has shown that for 60° and 70°, the probability is the lowest when comparing to other angles, while the drop height of 30 m was always dangerous when considering IMO's criteria. Another aspect of kinematics was how well a lifeboat can escape the hazardous event without extra propulsion, which would require time until the given acceleration turns into actual velocity. By this point of view, 70° was the one that performed the best, whereas 10°, the least, showing how effective can be the submergence phase.

In general, the project has shown that OpenFOAM is a robust tool to deal with slamming problems and can be used not only to measure the impact loads, but also to view the performance of the lifeboat when entering the water to flee from the hazardous event and save lives.

6 REFERENCES

Albadawi, A., Donoghue, D. B., Robinson , A. J., Murray, D. B., & Delauré, Y. M. (2013). Influence of surface tension implementation in Volume of Fluid and coupled Volume of Fluid with Level Set methods for bubble growth and detachment. International Journal of Multiphase Flow, 53, 11-28. doi:10.1016/j.ijmultiphaseflow.2013.01.005

Benites-Munoz, D., Huang, L., Anderlini, E., Marín-Lopez, J. R., & Thomas, G. (2020). Hydrodynamic Modelling of An Oscillating Wave Surge Converter Including Power Take-Of. Journal of Marine Science and Engineering, 8(10), 771. doi:10.3390/jmse8100771

Berton, A., D'Orrico, F., & Sideri, M. (2017). Overset grids for fluid dynamics analysis of internal combustion engines. Energy Procedia, 126, 979-986. doi:10.1016/j.egypro.2017.08.240

Duraisamy, K., Iaccarino, G., & Xiao, H. (2019). Turbulence Modeling in the Age of Data. Annual Review of Fluid Mechanics, 51(1), 357-377. doi:10.1146/annurev-fluid-010518-040547

Greenshields, C. J. (2015, May 21). OpenFOAM, The open source CFD Toolbox. User Guide.

Huang, L., Tavakoli, S., Li, M., Dolatshah, A., Pena, B., Ding, B., & Dashtimanesh, A. (2021). CFD analyses on the water entry process of a freefall lifeboat. Ocean Engineering, 232, 109115. doi:10.1016/j.oceaneng.2021.109115

IMO. (1991, November 6). Resolution A.689. IMO.

ITTC. (2017). Uncertainty Analysis in CFD Verification and Validation, Methodology and Procedures. ITTC Quality System Manual Recommended Procedures and Guidelines.

Kárman, T. v. (1929). The impact on seaplane floats during landing. Washington, DC;: National Advisory Committee for Aeronautics.

Kauczynski, W. E., Werenskiold, P., & Narten, F. (2009). Documentation of operational limits of free-fall lifeboats by combining model tests, full-scale tests, and computer simulation. Proceedings of the ASME 2009 28th International Conference on Ocean, Offshore and Artic Engineering. Volume 2: Structures, Safety and Reliability, 2. doi:10.1115/OMAE2009-79959

Liao, K., Hu, C., & Sueyoshi, M. (2015). Free surface flow impacting on an elastic structure: Experiment versus numerical simulation. In Applied Ocean Research (Vol. 50, pp. 192–208). Elsevier BV. https://doi.org/10.1016/j.apor.2015.02.002

Lopez Mejia, O. D., Mejia, O. E., Escorcia, K. M., Suarez, F., & Laín, S. (2021). Comparison of Sliding and Overset Mesh Techniques in the Simulation of a Vertical Axis Turbine for Hydrokinetic Applications. Processes, 1933. doi:10.3390/pr9111933

Muzaferija, S. (1998). A two-fluid Navier-Stokes solver to simulate water entry. Proceeding of the 22nd symposium of naval hydrodynamics.

Netherlands Regulatory Framework - Maritime. (1993, 06 22). 616 Evaluation of Free-fall Lifeboats launch performance. Retrieved from Netherlands Regulatory Framework (NeRF) – Maritime: https://puc.overheid.nl/nsi/doc/PUC_1746_14/1/

Oberhagemann, J. (2016). On Prediction of Wave-Induced Loads and Vibration of Ship Structures with Finite Volume Fluid Dynamic Methods. Duisburg: Doctoral Dissertation.

Pearce, C. (2020, April 22). BBC Science Focus Magazine. Retrieved from BBC Science Focus Magazine: https://www.sciencefocus.com/science/whats-the-maximum-speed-a-human-can-withstand/

Qiu, S., Ren, H., & Li, H. (2020, August). Computational Model for Simulation of Lifeboat Free-Fall during Its Launching from Ship in Rough Seas. Journal of Marine Science and Engineering, 8, 631. doi:10.3390/jmse8090631

Review of code and solution verification procedures for computational simulation. (2005). Journal of Computational Physics, 205(1), 131-156. doi:10.1016/j.jcp.2004.10.036

Ringsberg, J. W., Heggelund, S., Lara, P., Jang, B.-S., & Hirdaris, S. E. (2017). Structural response analysis of slamming impact on free fall lifeboats. Marine Structures, 54, 112-126. doi:10.1016/j.marstruc.2017.03.004

Roache, P. J. (1998). Criticisms of the "Correction Factor" Verification Method. Journal of Fluids Engineering, 125(4), 732-733. doi:10.1115/1.1588693

Roache, P. J. (2003). Criticism of the Correction Factor Verification Method. ASME J. Fluid Eng., 125(4), 732-733. doi:10.1115/1.1588693

Shen, Z., Hsieh, Y.-F., Ge, Z., Korpus, R., & Huan, J. (2016). Slamming Load Prediction Using Overset CFD Methods. Offshore Technology Conference. doi:10.4043/27254-MS

Sun, H., & Faltinsen, O. M. (2007). The influence of gravity on the performance of planing vessels in calm water. Journal of Engineering Mathematics, 58, 91-107. doi:10.1007/s10665-006-9107-5

Sun, P., Marrone, S., Ming, F., & Zhang, A.-M. (2018). An accurate and efficient SPH modeling of the water entry of circular cylinders. Applied Ocean Research, 72, 60-75. doi:10.1016/j.apor.2018.01.004

Tisovska, P. (2019). Description of the overset mesh approach in ESI version of OpenFOAM. In Proceedings of CFD with OpenSource Software. doi:10.17196/OS_CFD#YEAR_2019

Wagner, H. (1932). Über Stoß- und Gleitvorgänge an der Oberfläche von Flüssigkeiten. ZAMM - Zeitschrift für Angewandte Mathematik und Mechanik, 12(4), 193-215. doi:10.1002/zamm.19320120402

Wang, J., Lugni, C., & Faltinsen, O. M. (2015). Experimental and numerical investigation of a freefall wedge vertically entering the water surface. Applied Ocean Research, 51, 181-203. doi:https://doi.org/10.1016/j.apor.2015.04.003

Wang, S., & Guedes Soares, C. (2020). Effects of compressibility, three-dimensionality and air cavity on a free-falling wedge cylinder. Ocean Engineering, 217, 107-589. doi:10.1016/j.oceaneng.2020.107589

Wang, S., González-Cao, J., Islam, H., Gómez-Gesteira, M., & Guedes Soares, C. (2022). Uncertainty estimation of mesh-free and mesh-based simulations of the dynamics of floaters. Ocean Engineering, 256, 111386. doi:10.1016/j.oceaneng.2022.111386

Wang, S., Xiang, G., & Guedes Soares, C. (2021). Assessment of three-dimensional effects on slamming load predictions using OpenFoam. Applied Ocean Research, 112, 102646. doi:https://doi.org/10.1016/j.apor.2021.102646

Wu, G.-X., Xu, G.-D., & Duan, W.-Y. (2010). A summary of water entry problem of a wedge based on the fully nonlinear velocity potential theory. Journal of Hydrodynamics, 22(5), 859-864. doi:10.1016/S1001-6058(10)60042-X

Xiao, H., & Paola, C. (2019). Quantification of model uncertainty in RANS simulations: A review. Progress in Aerospace Sciences, 108, 1-31. doi:10.1016/j.paerosci.2018.10.001

Yettou, E.-M., Desrochers, A., & Champoux, Y. (2007). A new analytical model for pressure estimation of symmetrical water impact of a rigid wedge at variable velocities. Journal of Fluids and Structures, 23(3), 501-522. doi:10.1016/j.jfluidstructs.2006.10.001

Zhao, R., & Faltinsen, O. (1993). Water entry of two-dimensional bodies. Journal of Fluid Mechanics, 246, 593-612. doi:10.1017/S002211209300028X